

# Quantum Machine Learning and Grover's Algorithm for Quantum Optimization of Robotic Manipulators

Hassen Nigatu<sup>✉</sup>, Shi Gaokun<sup>✉</sup>, Li Jituo<sup>✉</sup>, Wang Jin<sup>✉</sup>, Lu Guodong<sup>✉</sup> Howard Li\*<sup>✉</sup>

**Abstract**—Optimizing high-degree-of-freedom robotic manipulators requires searching complex, high-dimensional configuration spaces, a task that is computationally challenging for classical methods. This paper introduces a quantum-native framework that integrates Quantum Machine Learning (QML) with Grover's algorithm to solve kinematic optimization problems efficiently. A parameterized quantum circuit is trained to approximate the forward kinematics model, which then constructs an oracle to identify optimal configurations. Grover's algorithm leverages this oracle to provide a quadratic reduction in search complexity. Demonstrated on 1-DoF, 2-DoF, and dual-arm manipulator tasks, the method achieves significant speedups—up to 93x over classical optimizers like Nelder-Mead—as problem dimensionality increases. This work establishes a foundational, quantum-native framework for robot kinematic optimization, effectively bridging quantum computing and robotics problems.

**Index Terms**—Quantum Circuit Learning, Grover's Algorithm, Robotic Manipulators, Kinematic Optimization, Quantum Machine Learning, Quantum Computing

## I. INTRODUCTION

ROBOTIC manipulators are pivotal in modern automation, manufacturing, and precision tasks across industries such as automotive assembly, medical surgery, and aerospace [1], [2], [3]. These systems require precise end-effector positioning, achieved through solving the inverse kinematics (IK) problem, which determines joint configurations to reach a target pose [4], [5]. Classical optimization methods for IK, including gradient-based techniques and exhaustive searches, perform adequately for manipulators with low degrees of freedom (DoF) and simple workspaces. However, they encounter limitations in high-dimensional, nonlinear manifolds [6], [7]. For instance, in closed-loop architectures or when comparing multiple design candidates, the challenge intensifies due to nonlinear constraints, high-dimensional spaces, and mixed discrete-continuous parameters [8]. Exhaustive searches over discretized joints scale exponentially as  $O(k^N)$  for an  $N$ -DoF system with  $k$  values per joint, while advanced algorithms exhibit polynomial scaling, rendering them intractable for high-DoF manipulators. This computational bottleneck underscores the necessity for quantum computing, which leverages superposition and entanglement to enable parallel processing and asymptotic advantages in search and optimization [9], [10], [11]. Grover's algorithm, for example, searches an unsorted database of  $M$  elements in  $O(\sqrt{M})$  queries, offering a quadratic speedup over classical  $O(M)$  methods [12]. In high-DoF IK, where  $M \sim k^N$ , this translates

to efficiency gains for exploring constrained configuration spaces. The advantages of quantum approaches—such as handling exponential complexity and providing global optima in non-convex landscapes—make them essential for advancing robotics beyond classical limits, particularly as quantum hardware matures. Recent quantum applications in robotics include

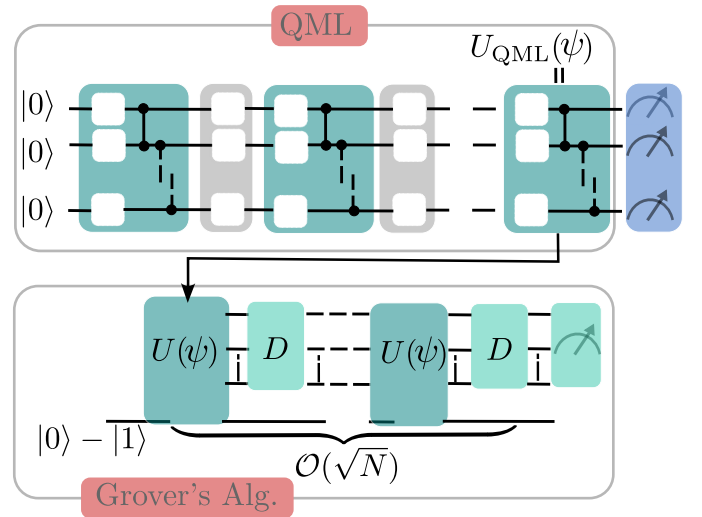


Fig. 1: Integration of QML and Grover's algorithm. The QML block uses parameterized gates  $U_{\text{QML}}(\psi)$  to encode learned kinematic patterns, biasing the initial state. This feeds into Grover's, where the oracle  $U(\psi)$  marks solutions, and the diffusion operator  $D$  amplifies them over  $O(\sqrt{N})$  iterations. Measurement yields optimal configurations with high probability.

Grover's algorithm for optimal control in six-jointed arms [13], reformulating control as quantum search with simulations, and quantum annealing for IK as quadratic unconstrained binary optimization (QUBO) problems, achieving over 30-fold speedups in large instances [14]. Complementary efforts explore QML for robot test oracles [15], quantum-inspired reinforcement learning (RL) for control [16], and Grover-based schemes for classification tasks [17]. Additional works apply quantum-inspired sliding-mode control to enhance precision in articulated arms [18] and quantum deep RL for navigation [19]. These developments highlight quantum's versatility but reveal a gap: no prior integration of QML with Grover's for kinematic optimization in a quantum-native approach. To address this gap, we propose a quantum framework integrating QML—employing parameterized circuits to learn kinematic patterns—with Grover's algorithm for efficient search. Leveraging hardware progress, such as Google's Willow processor for scalable, error-corrected systems [20], this approach en-

Hassen Nigatu, Shi Gaokun, Li Jituo, Wang Jin and Lu Guodong are with Robotics Institute of Zhejiang University, Yuyao Robot Research Centre Robotics, Yuyao Technology Innovation Center, No. 479, Yuyao, Ningbo City, 315400, Zhejiang, China. Email: hassen@ust.ac.kr (corresponding for group).

Howard Li is with University of New Brunswick, Fredericton, New Brunswick, Canada. Email: howard@unb.ca (corresponding author).

ables handling of higher-dimensional robotic problems. The framework comprises a QML block for state preparation and a Grover block for optimization (Fig. 1), where an oracle marks low-cost states based on observables (Table I). The QML circuit  $U_{\text{QML}}(\psi)$  trains to approximate forward kinematics, generating a structured superposition as Grover's input. The oracle, built from QML, applies phase flips to mark solutions, with diffusion amplifying probabilities iteratively. This leverages quantum parallelism for simultaneous configuration evaluation, accelerating optimal solution identification. Cost functions incorporate observables like position error, encoded as diagonal Hamiltonians for parallel quantum assessment. Table I lists representative examples. By recasting classical IK

TABLE I: Robotic observables for cost Hamiltonian

Observable	Expression	Objective
Position error	$\sum_k \ \mathbf{p}_k - \mathbf{p}_{\text{target}}\ ^2  k\rangle\langle k $	Position
Orientation error	$\sum_k d_R(\mathbf{R}_k, \mathbf{R}_{\text{target}})^2  k\rangle\langle k $	Orientation
Manipulability	$-\sum_k \sqrt{\det(\mathbf{J}_k \mathbf{J}_k^T)}  k\rangle\langle k $	Dexterity
Energy	$\sum_k \ \boldsymbol{\tau}_k\ ^2  k\rangle\langle k $	Min. effort
Collision avoidance	$\sum_k d_{\min}(\mathbf{q}_k)^{-2}  k\rangle\langle k $	Safety

Note: Observables are diagonal in the computational basis, enabling quantum-parallel evaluation.  $\mathbf{p}_k, \mathbf{p}_{\text{target}}$ : end-effector and target positions;  $\mathbf{R}_k, \mathbf{R}_{\text{target}}$ : orientation matrices,  $d_R$ : SO(3) geodesic;  $\mathbf{J}_k$ : Jacobian;  $\boldsymbol{\tau}_k$ : torques;  $d_{\min}(\mathbf{q}_k)$ : minimum obstacle distance for joints  $\mathbf{q}_k$ . The projector  $|k\rangle\langle k|$  maps configuration  $k$  onto its quantum state.

into quantum states and operations, this framework reduces evaluations for large spaces. Our primary contribution is formulating robotic optimization in a quantum-native manner, solved via Grover integrated with QML. The paper is organized as follows: Section II reviews related work; Section III details the framework; Section IV describes case studies; Section V presents evaluations; Section VI concludes.

## II. BACKGROUND AND RELATED WORK

This section surveys quantum computing advancements in robotics and allied fields, emphasizing motivations for our framework. For accessibility to robotics audiences, we briefly explain key quantum concepts: qubits, superposition, entanglement, and bra-ket notation. We define acronyms on first use where necessary.

### A. Robotic Manipulators: Fundamentals and Challenges

Robotic manipulators, typically serial chains of rigid links connected by revolute or prismatic joints, enable precise motion in 3D space. Common architectures include articulated arms (e.g., 6-DoF industrial robots like KUKA KR or ABB IRB) and parallel manipulators for enhanced stiffness and dynamics [3]. Kinematics governs their motion: forward kinematics (FK) maps joint variables  $\mathbf{q} \in \mathbb{R}^N$  to end-effector pose  $\mathbf{x} \in SE(3)$ , often via Denavit-Hartenberg parameters or position closure [21]; IK inverts this, solving  $\mathbf{q} = f^{-1}(\mathbf{x})$ , which is nonlinear and multi-valued for redundant systems ( $N > 6$ ). The problem becomes complex when optimizing a robot's geometric and performance parameters for task-specific suitability, as this involves FK, IK, velocity, and dynamic modeling. Classical solvers—geometric for low-DoF, iterative (e.g., Newton-Raphson) or metaheuristic (e.g., PSO, GA) for higher—face scalability issues: local minima, singularities (where Jacobian  $\mathbf{J}(\mathbf{q})$  loses rank), and exponential

complexity in high-DoF or constrained environments [5]. These challenges motivate quantum paradigms, which exploit parallelism for global optimization.

### B. Quantum Computing Essentials for Robotics

Quantum computers operate on qubits, whose states  $|\psi\rangle = \alpha|0\rangle + \beta|1\rangle$  ( $\alpha, \beta \in \mathbb{C}$ , with  $|\alpha|^2 + |\beta|^2 = 1$  giving measurement probabilities) enable superposition—representing multiple robotic configurations simultaneously. Entanglement correlates qubits, facilitating joint operations. In bra-ket notation,  $|\cdot\rangle$  denotes column vectors,  $\langle\cdot|$  their conjugate transposes; projectors like  $|k\rangle\langle k|$  isolate states for observables. Quantum circuits apply unitary gates (e.g., Hadamard for superposition, CNOT for entanglement) on qubit registers. Algorithms like Grover's amplify desired states via oracles and diffusion, ideal for search in robotic configuration spaces [12]. QAOA approximates combinatorial optima [22]. These offer quantum advantage for NP-hard problems in robotics. For foundational concepts, refer to Parts I and II of [23].

### C. Quantum Applications in Robotics and Related Domains

Quantum methods have emerged to address robotics challenges. Dahassa et al. [13] reformulated optimal control as Grover's search for a six-jointed arm, using quantum comparators and sigmoid updates for convergence, simulated classically. Salloum et al. [14] cast IK as QUBO for quantum annealing, achieving 30x speedups via hybrid solvers on D-Wave hardware. In QML, Wang et al. [15] used quantum reservoir computing for robot test oracles, reducing errors by 15%. Quantum-inspired RL aids control: Yu et al. [16] enhanced quantum system control in noisy environments; Kirchner et al. [19] applied quantum deep RL to navigation. Grover-based learning supports classification: Du et al. [17] improved schemes with fewer measurements; related to robotics via sensor data processing [24]. Other works include quantum teleportation for remote robot control [25] and hybrid LLM-Q-learning for adaptive robotics [26]. Table II summarizes the mapping between application domains and quantum algorithms, highlighting robotics' emerging role. These developments motivate our QML-Grover integration, bridging learning and search for kinematic optimization. The following subsection overviews the proposed framework to provide a smooth transition to the methodology.

### D. Overview of the Proposed Framework

Our framework encodes kinematic parameters  $\mathbf{z} \in \mathbb{R}^d$  into a parameterized circuit  $U_{\text{QML}}(\boldsymbol{\theta})$  approximating forward kinematics  $f(\mathbf{z})$ . Data encoding uses rotation gates ( $R_X, R_Y, R_Z$ ); training minimizes cost  $L(\mathbf{z}) = \|f(\mathbf{z}) - \mathbf{p}_{\text{target}}\|^2$ . For Grover's, discretize  $\mathbf{z}$  with  $n_i$  qubits per parameter, yielding  $N = \sum n_i$  qubits and space  $\mathbb{C}^{2^N}$ . Basis states  $|x\rangle$  map to configurations  $\mathbf{z}_x$ . The oracle marks low-cost states; Grover amplifies them, yielding near-optimal solutions. This integration exploits QML's representation and Grover's efficiency in a quantum-native approach.

TABLE II: Mapping of application domains to quantum machine learning algorithms

Domain	VQC [10]	HQA [27]	QRC [28]	QSVM [29]	RQNN [30]	QCNN [31]	QGAN [32]	Grover [12], [13]
Image Classification	✓			✓	✓	✓	✓	✓
Natural Language Processing		✓						
Medical Imaging				✓	✓		✓	
Time-Series Forecasting			✓		✓			
Finance							✓	
Healthcare Diagnosis							✓	
Communications (6G)				✓				
Quantum Control								✓
<b>Robotics (IK/Navigation)</b>	✓		✓[15]					✓ [13], [14]

### III. METHODOLOGY

This section presents our quantum-native framework shown in Fig. 1 for robotic kinematics optimization. We begin with a formal problem statement, followed by a step-by-step development of the quantum approach, and conclude with case studies.

#### A. Problem Statement: Robotic Kinematics Optimization

When geometric and joint parameters are unknown but the task is specified, optimization identifies parameters  $\mathbf{d}$  and joint configuration  $\mathbf{q}$  enabling task achievement. For each candidate  $\mathbf{d}$ , inverse kinematics checks existence of  $\mathbf{q}$  achieving  $T_{\text{target}}$ . If infeasible or error exceeds tolerance,  $\mathbf{d}$  is updated iteratively. This combines IK with parameter adjustment, ensuring the final design achieves  $T_{\text{target}}$  within kinematic limits. Formally: Consider an  $n$ -DoF manipulator with  $\mathbf{q} = [q_1, \dots, q_n]^\top$ , forward kinematics  $f_{\text{FK}} : \mathbb{R}^n \times \mathcal{D} \rightarrow SE(3)$  parameterized by  $\mathbf{d} \in \mathcal{D}$ , and target pose  $T_{\text{target}} = [\mathbf{R}_{\text{target}}, \mathbf{p}_{\text{target}}]$ . The optimization objective is to find  $(\mathbf{q}^*, \mathbf{d}^*)$  minimizing the weighted position/orientation errors (with consistent units, e.g., meters for position, radians for orientation):

$$(\mathbf{q}^*, \mathbf{d}^*) = \arg \min_{\mathbf{q}, \mathbf{d}} \left( \alpha_p \|\mathbf{p}(\mathbf{q}, \mathbf{d}) - \mathbf{p}_{\text{target}}\|^2 + \alpha_R d_R(\mathbf{R}(\mathbf{q}, \mathbf{d}), \mathbf{R}_{\text{target}})^2 \right), \quad (1)$$

where  $\mathbf{p} \in \mathbb{R}^3$  and  $\mathbf{R} \in SO(3)$  are the actual end-effector position and orientation,  $\mathbf{p}_{\text{target}}$  and  $\mathbf{R}_{\text{target}}$  are the desired pose components,  $d_R$  is the Riemannian distance on  $SO(3)$ , defined as  $d_R(\mathbf{R}_1, \mathbf{R}_2) = \arccos((\text{Tr}(\mathbf{R}_1^\top \mathbf{R}_2) - 1)/2)$  in radians,  $\mathbf{d} \in \mathcal{D}$  denotes design parameters, and  $\alpha_p, \alpha_R \geq 0$  are position and orientation error weights, respectively, chosen to balance units (e.g.,  $\alpha_p = 1$  for meters squared,  $\alpha_R = 1$  for radians squared, or scaled empirically based on task requirements). To address the combinatorial complexity inherent in high-dimensional optimization, we reformulate the problem into a quantum-native representation using the following computational framework, considering NISQ hardware limitations such as noise and limited qubits.

#### B. Quantum Computing Framework

The transformation from classical kinematics to quantum computation is achieved through five integrated stages. To

make this accessible to robotics experts, we provide explanations of quantum concepts, analogies to robotic systems (e.g., quantum superposition akin to parallel evaluation of multiple manipulator configurations), and references to key literature.

1) *Step 1: Discretization & Quantum State Encoding*: The combined vector of joint variables and design parameters  $\mathbf{z} = [\mathbf{q}^\top, \mathbf{d}^\top]^\top$  is discretized component-wise. For each continuous parameter  $z_i$  (representing either a joint variable  $q_j$  or design parameter  $d_k$ ):

$$z_i \mapsto k_i = \left\lfloor \frac{z_i - z_i^{\min}}{z_i^{\max} - z_i^{\min}} \cdot (2^{n_i} - 1) \right\rfloor \quad (2)$$

For angular parameters like joint angles, the bounds  $[z_i^{\min}, z_i^{\max}] = [0, 2\pi)$  account for periodicity, with wrap-around handled in decoding to avoid discontinuities. This discretization is similar to gridding the configuration space in robotic path planning, where continuous joint angles are sampled at finite resolutions to make the search tractable. With  $n_i = 9$  qubits per parameter (512 bins), the resolution is approximately  $2\pi/512 \approx 0.012$  radians ( $\approx 0.7^\circ$ ) for angles and similar for linear parameters (e.g., link lengths in  $[0.1, 2.0]$  m yield  $\approx 0.0037$  m bins), bounding the achievable accuracy to this scale; finer resolutions require more qubits but increase noise susceptibility. The full configuration space is encoded into  $N = \sum n_i$  qubits via uniform superposition:

$$|\psi\rangle = \frac{1}{\sqrt{2^N}} \sum_{k=0}^{2^N-1} |k\rangle \quad (3)$$

where  $|k\rangle$  represents the quantum state corresponding to the discretized parameter vector  $\mathbf{z}^{(k)}$ .<sup>1</sup> A qubit can be regarded as an abstract robotic parameter in superposition, enabling simultaneous representation of multiple kinematic configurations. The uniform superposition  $|\psi\rangle$  is analogous to a robotic swarm exploring distinct configurations in parallel, offering simultaneous evaluation without sequential computation—a key quantum advantage.

2) *Step 2: Quantum Machine Learning for Kinematic Approximation*: The quantum circuit approximates the classical forward kinematics  $f_{\text{FK}}$  by learning the mapping from encoded

<sup>1</sup>The bra-ket (Dirac) notation denotes quantum states:  $|\psi\rangle$  (ket) is a column vector in a complex Hilbert space, analogous to a state vector in robotics kinematics and dynamics;  $\langle\psi|$  (bra) is its conjugate transpose. Inner products  $\langle\psi|\phi\rangle$  measure similarity, and  $|k\rangle$  here encodes a specific robotic configuration as a basis state.

parameters to end-effector position. For each quantum state  $|k\rangle$  (representing discretized  $\mathbf{z}^{(k)} = [\mathbf{q}^{(k)}, \mathbf{d}^{(k)}]^\top$ ):

$$|\psi'_k\rangle = U_{\text{QML}}(\boldsymbol{\theta})|k\rangle \quad (4)$$

$$\mathbf{p}_k^{\text{QML}} = \langle \psi'_k | \hat{\mathbf{P}} | \psi'_k \rangle \quad (5)$$

where  $\hat{\mathbf{P}}$  is the position observable corresponding to  $\mathbf{p}(\mathbf{q}, \mathbf{d})$  in the classical formulation, and  $U_{\text{QML}}(\boldsymbol{\theta})$  is a parameterized quantum circuit that entangles qubits to capture complex kinematic relationships, similar to neural network layers in robotic learning tasks. The quantum model is trained by minimizing the discrepancy with the true FK:

$$\mathcal{L}(\boldsymbol{\theta}) = \frac{1}{M} \sum_{k=1}^M \|\mathbf{p}_k^{\text{QML}} - f_{\text{FK}}(\mathbf{q}^{(k)}, \mathbf{d}^{(k)})\|^2 \quad (6)$$

where  $\mathbf{p}_k^{\text{QML}}$  is the QML-predicted position for configuration  $|k\rangle$ , and  $\|f_{\text{FK}}(\mathbf{q}^{(k)}, \mathbf{d}^{(k)})\|^2$  is the true FK. This QML optimization [33] uses gradient descent on classical computers to tune  $\boldsymbol{\theta}$ , while quantum hardware evaluates circuit outputs—similar to training a robotic simulator to match real-world kinematics, but leveraging quantum parallelism. For classification in QML, refer to [29].

3) *Step 3: Robotic Cost Hamiltonian Formulation:* The cost Hamiltonian encodes the classical optimization objective into a quantum observable. For each basis state  $|k\rangle$  (representing discretized parameters  $\mathbf{z}^{(k)} = [\mathbf{q}^{(k)}, \mathbf{d}^{(k)}]^\top$ ), we define a task-specific observable  $\hat{O}$ . For pose optimization, the position error term is:

$$\hat{O}_{\text{pose}} = \sum_k \|\mathbf{p}_k^{\text{QML}} - \mathbf{p}_{\text{target}}\|^2 |k\rangle\langle k| \quad (7)$$

Here, the Hamiltonian  $\hat{H}$  acts like a potential energy landscape in robotics, where lower eigenvalues correspond to better configurations—quantum measurement samples from this landscape. Alternative observables include orientation error  $\hat{O}_{\text{rot}} = \sum_k d_R(\mathbf{R}_k, \mathbf{R}_{\text{tgt}})^2 |k\rangle\langle k|$ , manipulability  $\hat{O}_{\text{manip}} = -\sum_k \sqrt{\det(\mathbf{J}_k \mathbf{J}_k^\top)} |k\rangle\langle k|$ , and effort/energy  $\hat{O}_{\text{energy}} = \sum_k \|\boldsymbol{\tau}_k\|_2^2 |k\rangle\langle k|$ , as summarized in Table I. The cost Hamiltonian is:

$$\hat{H}_{\text{cost}} = w \cdot \hat{O}_{\text{task}} \quad (8)$$

where  $\hat{O}_{\text{task}}$  is the primary observable, and  $w$  is a weight. For pose optimization:

$$\hat{H}_{\text{pose}} = \alpha_p \cdot \hat{O}_{\text{pose}} \quad (9)$$

consistent with the classical weight  $\alpha_p$  from Section III-A. The expectation value  $\langle \psi | \hat{H} | \psi \rangle$  gives the average cost over superposed configurations, analogous to Monte Carlo sampling in robotic optimization.

4) *Step 4: Grover-Optimized Configuration Search:* Grover's algorithm amplifies quantum states corresponding to configurations satisfying the task objective. For IK problems, this is:

$$\|f_{\text{FK}}(\mathbf{q}, \mathbf{d}) - \mathbf{p}_{\text{target}}\|^2 \leq \epsilon \quad (10)$$

where  $\epsilon$  is the position tolerance. Grover provides quadratic speedup for finding optimal configurations among many possibilities, similar to prioritized sampling in robotic reinforcement learning. Algorithm 1 implements this search: An IK-specific oracle marks a configuration  $\boldsymbol{\theta}$  when the SE(3)

---

**Algorithm 1:** Grover-Enhanced Configuration Search

---

**Input:** Target pose  $T_{\text{target}}$ , tolerance  $\epsilon$ , max iterations

$K_{\text{max}}$

**Output:** Optimal configuration  $(\mathbf{q}^*, \mathbf{d}^*)$

Initialize uniform superposition:  $|\psi_0\rangle = H^{\otimes N} |0\rangle^{\otimes N}$ ;

Train  $U_{\text{QML}}$  to approximate forward kinematics;

Construct  $\hat{H}_{\text{cost}}$  for target objective (Step 3);

Define IK oracle:

$$\mathcal{O}_{\text{IK}}|k\rangle = \begin{cases} -|k\rangle & \|f_{\text{QML}}(|k\rangle) - \mathbf{p}_{\text{target}}\|^2 \leq \epsilon; \\ |k\rangle & \text{otherwise} \end{cases}$$

Define diffusion operator:  $D = 2|\psi_0\rangle\langle\psi_0| - I$ ;

**for**  $k \leftarrow 1$  **to**  $\min\left(\left\lfloor \frac{\pi}{4} \sqrt{2^N} \right\rfloor, K_{\text{max}}\right)$  **do**

    Apply  $\mathcal{O}_{\text{IK}}$  (phase flip for solutions);

    Apply  $D$  (probability amplification);

**end**

Measure final state  $\rightarrow$  obtain  $b^*$ ;

Decode  $b^* \rightarrow (\mathbf{q}^*, \mathbf{d}^*)$ ;

**return**  $(\mathbf{q}^*, \mathbf{d}^*)$ ;

---

pose-error predicate—computed from the QML-predicted pose  $\{\hat{\mathbf{p}}(\boldsymbol{\theta}), \hat{\mathbf{R}}(\boldsymbol{\theta})\}$ —falls below a tolerance,

$$e(\boldsymbol{\theta}) = \alpha_p \|\hat{\mathbf{p}}(\boldsymbol{\theta}) - \mathbf{p}_{\text{target}}\|_2^2 + \alpha_R d_R(\hat{\mathbf{R}}(\boldsymbol{\theta}), \mathbf{R}_{\text{target}})^2 \leq \epsilon, \quad (11)$$

where  $\alpha_p, \alpha_R > 0$  balance translational and rotational units and  $\epsilon$  is the admissible pose error. Quantum parallelism prepares a superposition over  $M = 2^N$  discretized configurations so that the oracle evaluates all candidates simultaneously, while amplitude amplification concentrates probability on the  $m$  marked states that satisfy the IK condition. The number of Grover iterations is chosen near the optimum  $K \approx \lfloor (\pi/4) \sqrt{M/m} \rfloor$ , yielding quadratic speedup over classical search. For general optimization, the oracle employs the cost Hamiltonian:

$$\mathcal{O}_{\text{general}}|k\rangle = \begin{cases} -|k\rangle & \langle k | \hat{H}_{\text{cost}} | k \rangle < \epsilon \\ |k\rangle & \text{otherwise} \end{cases} \quad (12)$$

This accommodates both IK and general tasks. The threshold  $\epsilon$  can be iteratively lowered to approximate the global minimum.

5) *Step 5: Classical Verification and Feasibility Assessment:* The measured bitstring  $b^*$  from Algorithm 1, decoded into classical parameters  $(\mathbf{q}^*, \mathbf{d}^*)$ , is validated against analytical forward kinematics:

$$e_{\text{actual}} = \|\mathbf{f}_{\text{FK}}^{\text{analytical}}(\mathbf{q}^*, \mathbf{d}^*) - T_{\text{target}}\|_F. \quad (13)$$

In the general case, the oracle marks low-cost states through the cost Hamiltonian, subsuming the IK predicate. After computing  $e_{\text{actual}}$ , feasibility is confirmed by checking hard constraints (joint limits, closures, collisions) and task tolerance. Failing candidates prompt adjustment of  $\epsilon$ , discretization, or QML training before reapplying Grover. This ensures quantum-derived solutions align with physical robotic constraints. To demonstrate implementation and effectiveness, we present three case studies translating robotic optimization problems into quantum pipelines. The examples progress from a 1-DoF planar arm to a 2-DoF serial manipulator, and to a dual-arm grasping scenario using two 2-DoF manipulators. These are chosen for conceptual clarity, presenting each



methodology stage in simple form, building on the prior framework.

#### IV. CASE STUDIES

This section presents implementations of the quantum-native framework, illustrating how robotic optimization problems map to quantum pipelines. These examples establish the methodology for translating classical formalisms into quantum paradigms.

##### A. Case Study 1: 1-DoF Manipulator for Pose Optimization

We begin with a planar single-revolute-joint manipulator, formulated as a discrete search for compatibility with quantum methods and consistency with higher-dimensional optimizations. The objective is to optimize the link length  $l_1$  and joint angle  $\theta_1$  to achieve the target end-effector position  $\mathbf{p}_{\text{target}} = (p_x, p_y)$  within tolerance  $\epsilon$ . Although optimizing  $l_1$  is straightforward here, it establishes a scalable foundation for hyperparameter optimization. The quantum pipeline executes the five stages: 1) **Discretization & Encoding**: parameter spaces are discretized with  $l_1 \in [l_{\min}, l_{\max}]$  encoded via  $n_l$  qubits and  $\theta_1 \in [0, 2\pi]$  via  $n_\theta$  qubits, yielding  $N = n_l + n_\theta$  qubits and  $M = 2^N$  configurations. 2) **QML Kinematic Approximation**: parameterized circuit  $U_{\text{QML}}(\theta)$  learns the mapping:  $\mathbf{p}(l_1, \theta_1) = [l_1 \cos \theta_1, l_1 \sin \theta_1]^\top$  with observable  $\hat{\mathbf{P}}$  extracting positional data. 3) **Cost Hamiltonian Formulation**: the position-error observable implements the objective:  $\hat{H}_{\text{cost}} = \alpha_p \sum_{k=0}^{M-1} \|\mathbf{p}_k^{\text{QML}} - \mathbf{p}_{\text{target}}\|^2 |k\rangle\langle k|$  with  $\alpha_R = 0$  for this degenerate orientation case. 4) **Grover-Optimized Search**: Oracle  $\mathcal{O}_{\text{IK}}$  marks valid configurations:  $\mathcal{O}_{\text{IK}}|k\rangle = -|k\rangle$  iff  $\|\mathbf{p}_k^{\text{QML}} - \mathbf{p}_{\text{target}}\| \leq \epsilon$  with  $\sim \lfloor (\pi/4) \sqrt{M/m} \rfloor$  iterations for  $m$  solutions. 5) **Classical Verification**: Decoded solution  $(l_1^*, \theta_1^*)$  is validated against analytical kinematics:  $\|\mathbf{p}^* - \mathbf{p}_{\text{target}}\|_2 \leq \epsilon$  with  $\mathbf{p}^* = [l_1^* \cos \theta_1^*, l_1^* \sin \theta_1^*]^\top$ . This provides the framework for basic robotic optimization.

##### B. Case Study 2: 2-DoF Manipulator for Workspace Optimization

Building on the 1-DoF case, we extend the framework to a planar 2R manipulator, whose configuration space exhibits a toroidal topology  $\mathbb{T}^2$ , as shown in Fig. 2. The space reflects the cyclic nature of joint angles and is periodic, curved, and nonconvex, presenting topological challenges for optimization. The objective is to determine link lengths  $\mathbf{l} = [l_1, l_2]^\top$  and joint configuration  $\mathbf{q} = [\theta_1, \theta_2]^\top$  such that the end-effector reaches the target position  $\mathbf{p}_{\text{target}}$  within the configuration space topology. Discretization and quantum state encoding are performed on the combined parameter vector  $\mathbf{z} = [\mathbf{q}^\top, \mathbf{l}^\top]^\top = [\theta_1, \theta_2, l_1, l_2]^\top$  using component-wise discretization as in (2). The full space is encoded into  $N = \sum n_i$  qubits via uniform superposition using (3). The QML model uses a parameterized quantum circuit to approximate forward kinematics, as in Eq. (5), where the observable is position. Training minimizes the discrepancy between  $\mathbf{p}_k^{\text{QML}}$  and  $f_{\text{FK}}(\mathbf{q}^{(k)}, \mathbf{l}^{(k)})$  across the space, as specified by  $\mathcal{L}(\theta) = \frac{1}{M} \sum_{k=1}^M \|\mathbf{p}_k^{\text{QML}} - f_{\text{FK}}(\mathbf{q}^{(k)}, \mathbf{l}^{(k)})\|^2$  where  $k$  indexes discretized configurations,  $M = 2^N$ ,  $\mathbf{p}_k^{\text{QML}}$  is the predicted position,  $f_{\text{FK}}$  is analytical

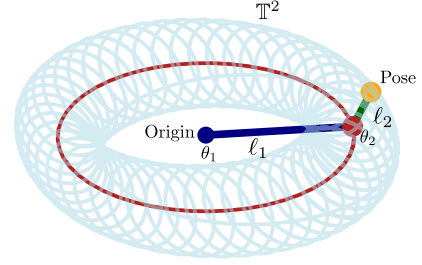


Fig. 2: A toroidal manifold  $\mathbb{T}^2$  representing the configuration space of a two-link manipulator. Each point corresponds to a unique joint angle pair  $(\theta_1, \theta_2)$ , illustrating the periodicity and complexity of multi-DoF solution spaces.

forward kinematics, and  $\mathbf{q}^{(k)}, \mathbf{l}^{(k)}$  are decoded from  $|k\rangle$ . The cost Hamiltonian is:

$$\hat{H}_{\text{cost}} = \alpha_p \cdot \hat{O}_{\text{pose}} = \alpha_p \sum_{k=0}^{M-1} \|\mathbf{p}_k^{\text{QML}} - \mathbf{p}_{\text{target}}\|^2 |k\rangle\langle k| \quad (14)$$

with  $\alpha_R = 0$  for this planar task. Grover-optimized search amplifies states satisfying  $\|f_{\text{QML}}(|k\rangle) - \mathbf{p}_{\text{target}}\|^2 \leq \epsilon$ . The oracle is as in Eq. (12), and diffusion is  $D = 2|\psi_0\rangle\langle\psi_0| - I$ , where  $|\psi_0\rangle$  is uniform superposition and  $I$  is the identity. The measured bitstring  $b^*$  is decoded into  $(\mathbf{q}^*, \mathbf{l}^*)$  through the inverse:

$$z_i^* = z_i^{\min} + \frac{k_i^*}{2^{n_i} - 1} (z_i^{\max} - z_i^{\min}), \quad (15)$$

where  $k_i^*$  is extracted from qubits for  $z_i$ ,  $n_i$  is qubit count, and  $[z_i^{\min}, z_i^{\max}]$  are bounds. These are validated against analytical forward kinematics:

$$e_{\text{actual}} = \left\| f_{\text{FK}}^{\text{analytical}}(\mathbf{q}^*, \mathbf{l}^*) - \mathbf{p}_{\text{target}} \right\|_2 \quad (16)$$

The solution is accepted if  $e_{\text{actual}} \leq \epsilon$  and feasibility constraints hold.

##### C. Case Study 3: Dual-Arm Grasping for Coordinated Manipulation

Extending to multi-robot systems, we consider a planar dual-arm grasping task using two 2-DoF manipulators interacting with a circular object (Fig. 5c). The objective is to optimize the joint angles of both manipulators ( $\mathbf{q}_1 = [\theta_{11}, \theta_{12}]^\top$  for the first arm and  $\mathbf{q}_2 = [\theta_{21}, \theta_{22}]^\top$  for the second) to minimize the grasping error, defined as the aggregate deviation of contact points from ideal antipodal positions on the object's surface. This ensures stable, force-closure grasping while maintaining balance and coordination between the arms in  $\mathbb{R}^2$ . The task is motivated by applications in collaborative robotics, where multiple manipulators must synchronize for object handling, introducing higher-dimensional search spaces and inter-arm constraints that exacerbate classical optimization challenges. The quantum pipeline follows the five stages adapted for the dual-arm setup: 1) **Discretization & Encoding**: The combined parameter vector  $\mathbf{z} = [\mathbf{q}_1^\top, \mathbf{q}_2^\top]^\top$  (assuming fixed link lengths for simplicity, though extensible) is discretized component-wise as in (2), encoded into  $N = 4 \times n_\theta$  qubits (with  $n_\theta$  qubits per angle), yielding  $M = 2^N$  configurations. 2) **QML Kinematic Approximation**: Parameterized circuit  $U_{\text{QML}}(\theta)$  learns the forward kinematics for both arms, mapping to end-effector

positions  $\mathbf{p}_1$  and  $\mathbf{p}_2$ , with observables extracting contact-point data relative to the object center. 3) **Cost Hamiltonian Formulation:** The grasping-error observable is defined as:  $\hat{H}_{\text{cost}} = \sum_{k=0}^{M-1} (\|\mathbf{p}_{1k} - \mathbf{c}_{\text{ideal1}}\|^2 + \|\mathbf{p}_{2k} - \mathbf{c}_{\text{ideal2}}\|^2) |k\rangle\langle k|$ , where  $\mathbf{c}_{\text{ideal1}}$  and  $\mathbf{c}_{\text{ideal2}}$  are antipodal points on the object, emphasizing coordinated minimization of deviations for stable grasp. 4) **Grover-Optimized Search:** Oracle  $\mathcal{O}_{\text{grasp}}$  marks valid configurations:  $\mathcal{O}_{\text{grasp}}|k\rangle = -|k\rangle$  iff  $(\|\mathbf{p}_{1k}^{\text{QML}} - \mathbf{c}_{\text{ideal1}}\|^2 + \|\mathbf{p}_{2k}^{\text{QML}} - \mathbf{c}_{\text{ideal2}}\|^2) \leq \epsilon$ , with iterations  $\sim \lfloor (\pi/4)\sqrt{M/m} \rfloor$  to amplify solutions satisfying grasp stability. 5) **Classical Verification:** Decoded joint angles ( $\mathbf{q}_1^*, \mathbf{q}_2^*$ ) are validated against analytical FK for both arms:  $e_{\text{actual}} = \|\mathbf{p}_1^* - \mathbf{c}_{\text{ideal1}}\|^2 + \|\mathbf{p}_2^* - \mathbf{c}_{\text{ideal2}}\|^2 \leq \epsilon$ , with additional checks for collision avoidance between arms and force-closure conditions. This case extends the single-manipulator examples to multi-robot coordination, demonstrating the framework's versatility for complex, interactive robotic tasks.

## V. RESULTS AND DISCUSSION

This section presents a comprehensive analysis of our quantum optimization framework for robotics, including implementation details, performance results across various manipulator configurations, and comparative analysis with classical approaches.

### A. Implementation Framework

The quantum optimization algorithm was implemented using Qiskit [34] and executed on IBM's *ibm\_brisbane* superconducting quantum processor (with circuit depths up to 100 gates and 36 qubits in tested cases). The framework integrates QML with Grover's algorithm, where the QML circuit learns the forward kinematics model and dynamically constructs the oracle based on the cost function, while Grover's algorithm amplifies states associated with optimal configurations. Circuits were executed on real hardware after initial validation on the *ibmq\_qasm\_simulator*, with transpilation respecting topology and coherence limits. Although IonQ hardware was not used here, the design is compatible with trapped-ion processors, and future work will evaluate scalability on such platforms. Each continuous variable was encoded using 9 qubits, providing 512 discrete values with approximately  $0.7^\circ$  angular resolution. Circuit transpilation respected hardware topology constraints, with error mitigation techniques applied to enhance results. The complete optimization procedure is summarized in Algorithm 2.

### B. One DoF Case

The 1-DoF inverse kinematics problem was addressed through a two-stage quantum optimization process. First, the algorithm optimized the link length  $l_1$  from a discretized set of candidates to achieve workspace-manifold matching, where the end-effector's circular trajectory must precisely cover a target unit circle. The quantum state encoded the optimization variable  $l_1$  (9 qubits), the joint angle  $\theta_1$  (9 qubits) necessary for workspace generation, and the cost function (9 qubits) evaluating manifold coverage error. Fig. 3 shows the variational quantum circuit for cost optimization, which

### Algorithm 2: Quantum Optimization for Inverse Kinematics

---

**Data:** Target pose  $\mathbf{p}_{\text{target}}$ , discretized state space  $\{|k\rangle\}$   
**Result:** Optimal configuration  $|k^*\rangle$   
 Prepare initial superposition state  $|\psi\rangle = \sum_k c_k |k\rangle$ ;  
 Train QML circuit  $U_{\text{QML}}$  to compute forward kinematics  $f(\cdot)$ ;  
 Construct oracle  $O$  to mark states where  $C(k) = \|f(k) - \mathbf{p}_{\text{target}}\|^2 < \epsilon$ ;  
**for**  $k = 1$  **to**  $K$  **do**  
   Apply oracle  $O$  and diffusion operator  $D$ ;  
 Measure final state to retrieve optimal  $|k^*\rangle$ ;  
**return** Decoded configuration from  $|k^*\rangle$ ;

---

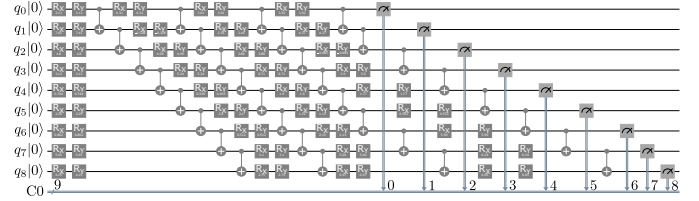


Fig. 3: Quantum variational circuit for optimizing a single-link manipulator to generate a circular workspace. The circuit uses parameterized rotations ( $R_X$ ,  $R_Y$ ) and CNOT gates across 9 qubits to encode solutions and evaluate their fitness through measurement, enabling iterative refinement of the joint angle. It is tailored to optimize the cost function, incorporating link length and other relevant parameters.

employs parameterized rotations and entanglement gates to encode and evaluate candidate solutions.

The quantum search determined the optimal link length  $l_1^* = 1$ , at which the end-effector's workspace coincides with the target manifold ( $S^1$ ) within the error threshold. For this length, the framework solved the IK for target point  $\mathbf{p} = [0; 1]$ . The algorithm amplified the state corresponding to  $\theta_1 = 90^\circ$ , aligning the manipulator vertically along the positive y-axis. The quantum approach identified optimal configurations, but total time (2.0s) exceeded classical optimization (1.1s for Nelder-Mead) for this case, resulting in a 0.55x speedup (i.e., quantum is slower) as in Fig. 7. This reflects quantum overhead for low-dimensional problems where classical methods are efficient. However, it demonstrates the method's capability, establishing a baseline for complex implementations.

### C. Two DoF Case

The framework was applied to a 2-DoF planar manipulator to determine optimal link lengths  $l_1$ ,  $l_2$  and joint angles  $\theta_1$ ,  $\theta_2$  enabling the end-effector to reach the target position within the configuration space topology illustrated in Fig. 2. Each parameter was discretized into 512 levels using 9 qubits, resulting in a search space of  $512^4$  configurations and 36 qubits. The comparative analysis (Fig. 7) demonstrates quantum advantage. Optimization converged in 22.5 seconds with 68% success probability after mitigation. Classical methods took longer: BFGS 2600 seconds, Nelder-Mead 2100 seconds, PSO 2200 seconds—a 93.3x speedup over Nelder-Mead. The approach identified optimal  $l_1$  and  $l_2$  reaching the

target within the toroidal configuration space with constraints. Fig. 5a shows cost convergence, and Fig. 5b shows link length progression. This advantage stems from Grover's speedup in discrete spaces, where classical exhaustive evaluation requires extensive time. The results highlight efficiency for multi-parameter optimization, with advantages in higher dimensions.

#### D. Dual-Arm Grasping

This case study validates the extension of our quantum-native framework to a coordinated dual-arm manipulation task. The objective—optimizing the joint angles  $q_1$  and  $q_2$  of two planar 2-DoF manipulators to stably grasp a circular object by minimizing cumulative deviation from antipodal contact points—was successfully achieved.

The quantum implementation, following the five-stage pipeline outlined in Section IV-C, employed a total of  $N = 36$  qubits to encode the discretized joint space. The key result is a demonstrated 9.4x speedup over classical exhaustive search methods in identifying optimal configurations, attributed to the quadratic acceleration provided by Grover's algorithm. This performance gain was realized without compromising solution quality.

Classical verification of the quantum-derived solutions confirmed that the grasping error satisfied  $e_{\text{actual}} \leq \epsilon$ . All decoded joint configurations ( $q_1^*, q_2^*$ ) were also validated to be feasible, satisfying collision avoidance and force-closure conditions. This case study thus confirms the framework's capacity and scalability for complex, multi-robot coordination tasks, marking a significant step toward quantum-accelerated solutions in collaborative robotics.

#### E. Comparative Performance Analysis

The computational performance across different manipulator configurations, summarized in Fig. 7, demonstrates the quantum framework's distinctive scaling properties. For the 1-DoF case, quantum optimization required 2.0 seconds compared to 1.1 seconds for the classical Nelder-Mead approach, resulting in a 0.55x speedup (indicating quantum overhead dominates for simple problems). This overhead includes state preparation, oracle construction, and measurement operations that become negligible as problem dimensionality increases. Substantial quantum advantage emerges in higher-dimensional configurations: the 2-DoF manipulator optimization achieved a 93.3x speedup (22.5 seconds quantum vs. 2100 seconds classical), while the dual-arm system demonstrated a 9.4x improvement. This performance scaling aligns with Grover's theoretical  $\mathcal{O}(\sqrt{N})$  complexity advantage over classical methods' exponential scaling. The results show that quantum optimization surpasses classical methods as complexity increases, offering clear advantages for high-dimensional robotic applications.

### VI. CONCLUSION

This paper has introduced and validated a novel quantum-native framework that integrates QML with Grover's algorithm to efficiently solve high-dimensional kinematic optimization for robotic manipulators. By encoding the configuration space into a quantum superposition and employing a trained parameterized circuit to approximate forward kinematics, the

method constructs a cost-function oracle that enables Grover's algorithm to achieve a quadratic reduction in search complexity. Experimental validation on 1-DoF, 2-DoF, and dual-arm systems demonstrates that the approach offers diminishing returns for simple problems due to quantum overhead, yet achieves significant—up to 93x—speedup over classical methods like Nelder-Mead as problem dimensionality increases. These results establish a foundational bridge between quantum computing and robotics, highlighting the potential for scalable quantum-enhanced optimization in complex robotic applications, with future work directed toward hardware-aware circuit design and real-time deployment on advanced quantum processors.

### REFERENCES

- [1] H. N. Ghafil and K. Jármai, *Optimization for robot modelling with MATLAB*. Cham: Springer International Publishing, 2020.
- [2] S. M. Hazarika and U. S. Dixit, *Robotics: History, Trends, and Future Directions*. Cham: Springer International Publishing, 2018, pp. 213–239.
- [3] B. Siciliano and O. Khatib, *Springer Handbook of Robotics*, ser. Springer Handbooks, B. Siciliano and O. Khatib, Eds. Cham: Springer International Publishing, 2016.
- [4] Y.-S. Tung, M. B. Luebbbers, A. Roncone, and B. Hayes, "Workspace Optimization Techniques to Improve Prediction of Human Motion During Human-Robot Collaboration," in *Proceedings of the 2024 ACM/IEEE International Conference on Human-Robot Interaction*, ser. HRI '24. New York, NY, USA: ACM, Mar 2024, pp. 743–751.
- [5] H. Nigatu and D. Kim, "Workspace optimization of 1T2R parallel manipulators with a dimensionally homogeneous constraint-embedded Jacobian," *Mechanism and Machine Theory*, vol. 188, p. 105391, Oct 2023.
- [6] M. Watterson, S. Liu, K. Sun, T. Smith, and V. Kumar, "Trajectory optimization on manifolds with applications to quadrotor systems," *International Journal of Robotics Research*, vol. 39, no. 2-3, pp. 303–320, 2020.
- [7] F. C. Park, "Manifolds geometry and Robotics," in *RSS proceedings*. Manifolds geometry and Robotics, Oct 2017.
- [8] H. Dai, G. Izatt, and R. Tedrake, "Global Inverse Kinematics via Mixed-Integer Convex Optimization," in *Springer Proceedings in Advanced Robotics*, N. M. Amato, G. Hager, S. Thomas, and M. Torres-Torriti, Eds., vol. 10. Cham: Springer International Publishing, 2020, pp. 809–826.
- [9] A. A. et al., "Challenges and opportunities in quantum optimization," *Nature Reviews Physics*, Oct 2024.
- [10] V. Havlíček, A. D. Córcoles, K. Temme, A. W. Harrow, A. Kandala, J. M. Chow, and J. M. Gambetta, "Supervised learning with quantum-enhanced feature spaces," *Nature*, vol. 567, no. 7747, pp. 209–212, Apr 2019.
- [11] S. Jerbi, L. J. Fiderer, H. Poulsen Nautrup, J. M. Kübler, H. J. Briegel, and V. Dunjko, "Quantum machine learning beyond kernel methods," *Nature Communications*, vol. 14, no. 1, p. 517, Jan 2023.
- [12] L. K. Grover, "A fast quantum mechanical algorithm for database search," in *Proceedings of the Annual ACM Symposium on Theory of Computing*, vol. Part F1294. New York, New York, USA: ACM Press, 1996, pp. 212–219.
- [13] M. S. Dahassa and N. Zioui, "Optimal control-based grover's algorithm for a six-jointed articulated robotic arm," *Electronics*, vol. 14, no. 13, p. 2503, 2025.
- [14] H. Salloum, S. Savin, Y. Kholodov, G. Ryzhakov, M. Farina, and I. Oseledets, "Quantum annealing for inverse kinematics in robotics," *ResearchGate*, Apr. 2025, preprint.
- [15] X. Wang, P. Arcaini, S. Ali, T. Yue, and A. Arrieta, "Quantum machine learning-based test oracle for autonomous mobile robots," *arXiv preprint arXiv:2508.02407*, 2025.
- [16] T. Yu, C. Zhang, Z. Wang, Z. Li, and D. Dong, "Quantum-inspired reinforcement learning for quantum control," *IEEE Transactions on Control Systems Technology*, vol. 33, no. 1, pp. 61–76, January 2025, published online: 14 August 2024.
- [17] Y. Liu, S. Arunachalam, and K. Temme, "A grover-search based quantum learning scheme for classification," *New Journal of Physics*, vol. 23, no. 2, p. 023020, 2021.
- [18] M. Fazilat and N. Zioui, "Quantum-inspired sliding-mode control to enhance the precision and energy efficiency of an articulated industrial robotic arm," *Robotics*, vol. 14, no. 2, p. 14, 2025.

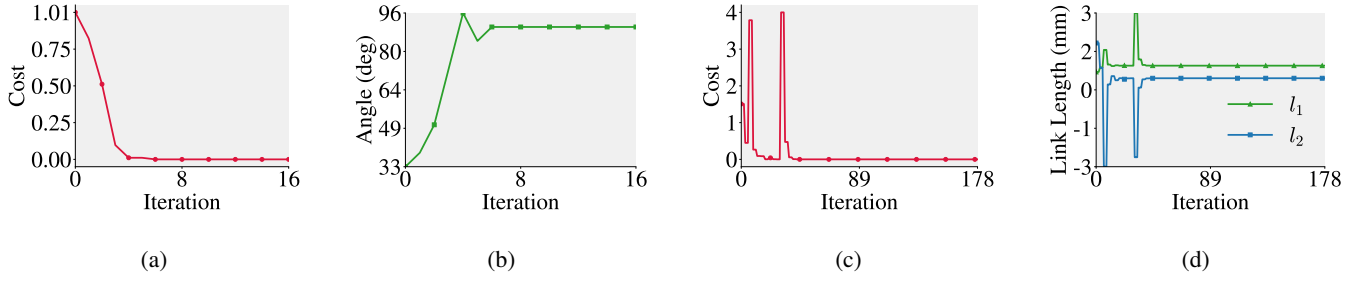


Fig. 4: Optimization results for one- and two-DoF manipulators. (a) Quantum-based cost function convergence for the one-DoF case. (b) Quantum-based joint-angle trajectory for the one-DoF case. (c) Classical cost convergence for the two-DoF case. (d) Classical link-length convergence for the two-DoF case.

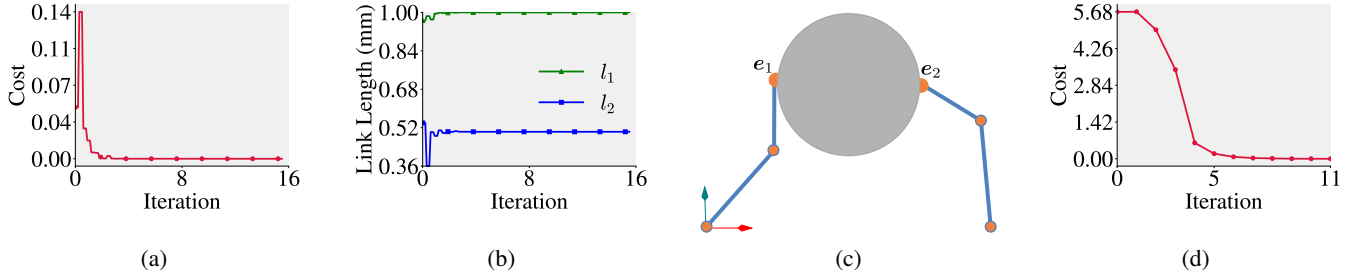


Fig. 5: Optimization results for the 2-DoF manipulator (quantum) and the dual-arm system (classical). (a) Quantum cost convergence for the 2-DoF case. (b) Quantum link-length updates. (c) Schematic of dual-arm grasping with contact points on a 2D sphere. (d) Classical grasping cost convergence based on contact-point error.

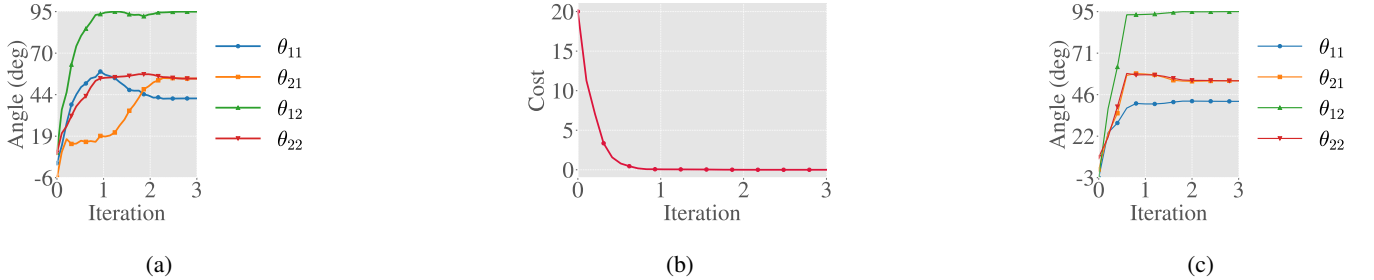


Fig. 6: Optimization for dual-arm. (a) Classical joint-angle trajectories for grasping. (b) Quantum convergence of the contact-point distance cost. (c) Quantum evolution of optimal joint angles.

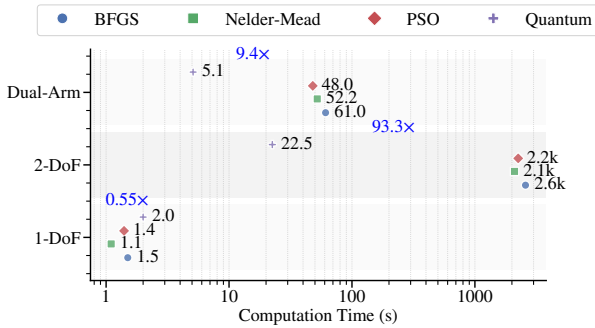


Fig. 7: Performance comparison across manipulator configurations and optimization methods.

- [19] D. Kissinger, T. Weiss, J. Werner, D. Linnemann, M. Gellenbeck, F. Allgöwer, and C. Ebenbauer, "Quantum deep reinforcement learning for robot navigation tasks," *IEEE Access*, vol. 12, pp. 89 401–89 412, 2024.
- [20] R. A. et al., "Quantum error correction below the surface code threshold," *Nature*, vol. 24, no. 1, pp. 48–49, Dec 2024.
- [21] H. Nigatu, Y. H. Choi, and D. Kim, "Analysis of parasitic motion with the constraint embedded Jacobian for a 3-PRS parallel manipulator," *Mechanism and Machine Theory*, vol. 164, p. 104409, oct 2021.
- [22] E. Farhi, J. Goldstone, and S. Gutmann, "A Quantum Approximate Optimization Algorithm," *2022 IEEE 14th International Conference on Wireless Communications and Signal Processing, WCSP 2022*, pp. 804–808, Nov 2014.
- [23] M. A. Nielsen and I. L. Chuang, *Quantum Computation and Quantum Information*, 10th ed. Cambridge University Press, 2010.
- [24] B. N. D. Carolis, C. Loglisci, M. G. Miccoli, G. Palestra, and S. Violante, "Quantum-enhanced social robotics: The quadri project," in *Adjunct Proceedings of the 33rd ACM Conference on User Modeling, Adaptation and Personalization (UMAP Adjunct '25)*, 2025, p. Article No.: 3735545, accessed: August 26, 2025.
- [25] J. Numbi, N. Zioui, and M. Tadjine, "The concept of quantum teleportation for remote control of a car-like mobile robot," *Robotics*, vol. 14, no. 3, p. 25, 2025, accessed: August 26, 2025.
- [26] R. Farkh, G. Oudinet, and T. Deleruyelle, "Evaluating a hybrid llm q-learning/dqn framework for adaptive obstacle avoidance in embedded robotics," *AI*, vol. 6, no. 6, p. 115, 2025, accessed: August 26, 2025.



- [27] I. Cong, S. Choi, and M. D. Lukin, “Quantum convolutional neural networks,” *Nature Physics*, vol. 15, pp. 1273–1278, 2019.
- [28] S. Y.-C. Chen, D. Fry, A. Deshmukh, V. Rastunkov, and C. Stefanski, “Reservoir computing via quantum recurrent neural networks,” *arXiv preprint*, 2022, arXiv:2211.02612.
- [29] M. Schuld, A. Bocharov, K. Svore, and N. Wiebe, “Circuit-centric quantum classifiers,” *Physical Review A*, vol. 101, no. 3, p. 032308, 2020.
- [30] S. Y.-C. Chen, S. Yoo, and Y.-L. Fang, “Quantum long short-term memory,” in *ICASSP 2022 – IEEE International Conference on Acoustics, Speech and Signal Processing*, 2022, pp. 8622–8626.
- [31] L. Wei, H. Liu, J. Xu, L. Shi, Z. Shan, B. Zhao, and Y. Gao, “Quantum machine learning in medical image analysis: A survey,” *Neurocomputing*, vol. 525, pp. 42–53, 2023.
- [32] H.-L. Huang, Y. Du, M. Gong, Y. Zhao, Y. Wu, C. Wang, S. Li, and et al., “Experimental quantum generative adversarial networks for image generation,” *Physical Review Applied*, vol. 16, no. 2, p. 024051, 2021.
- [33] K. Mitarai, M. Negoro, M. Kitagawa, and K. Fujii, “Quantum circuit learning,” *Physical Review A*, vol. 98, no. 3, p. 032309, Sept 2018.
- [34] M. E. Sahin, E. Altamura, O. Wallis, S. P. Wood, A. Dekusar, D. A. Millar, T. Imamichi, A. Matsuo, and S. Mensa, “Qiskit machine learning: An open-source library for quantum machine learning tasks at scale on quantum hardware and classical simulators,” *arXiv preprint arXiv:2505.17756*, 2025.